Received: 12 November 2020 | Revised: 13 June 2021 | Accepted: 5 July 2021

DOI: 10.1111/andr.13077

ANDROLOGY

WILEY

ORIGINAL ARTICLE

X-ray micro-computed tomography in the assessment of penile cavernous fibrosis in a rabbit castration model

Mikhail I. Kogan[1,§] | Igor V. Popov[1,2,§] | Evgeniya Y. Kirichenko[2,3,§] | Boris I. Mitrin[4] | Evgeniy V. Sadyrin[4] | Elizaveta D. Kulaeva[3] | Ilya V. Popov[1,2] | Sergey N. Kulba[2] | Alexander K. Logvinov[3] | Marina A. Akimenko[2,5] | Dmitry G. Pasechnik[2] | Sergey Yu. Tkachev[6] | Nikolay S. Karnaukhov[7] | Tatyana O. Lapteva[8] | Irina A. Sukhar[8] | Alexey Yu. Maksimov[8] | Alexey M. Ermakov[2]

[1] Department of Urology and Reproductive Health (with the Course of Pediatric Urology-Andrology), Rostov State Medical University, Rostov-on-Don, Russia

[2] Faculty of Bioengineering and Veterinary Medicine, Don State Technical University, Rostov-on-Don, Russia

[3] Academy of Biology and Biotechnology named after D. I. IvanovskySouthern Federal University, Rostov-on-Don, Russia

[4] Research and Education Centre "Materials", Don State Technical University, Rostov-on-Don, Russia

[5] Department of Medical Biology and Genetics, Rostov State Medical University, Rostov-on-Don, Russia

[6] Institute for Regenerative Medicine, Sechenov First Moscow State Medical University (Sechenov University), Moscow, Russia

[7] Moscow Clinical Research Center named after A. S. Loginov, Moscow, Russia

[8] National Medical Research Centre for Oncology, Rostov-on-Don, Russia

Correspondence
Igor V. Popov, Department of Biology and Pathonomy, Don State Technical University, Gagarin Square, 1, Rostov-on-Don, 344000, Russia.
Email: ipopov@donstu.ru

[§]These authors contributed equally to this work.

Abstract

Background: Current assessment methods of penile cavernous fibrosis in animal models have limitations due to the inability to provide complex and volume analysis of fibrotic alterations.

Objective: The aim was to evaluate micro-computed tomography for assessment of cavernous fibrosis and compare it with histological, histochemical, immunohistochemical, and RT-PCR analysis.

Materials and methods: A controlled trial was performed involving 25 New Zealand male rabbits with induced testosterone deficiency by orchidectomy. Penile samples were obtained before and after 7, 14, 21, and 84 days from orchidectomy. We consistently performed (a) gray value analysis of corpora cavernosa 3D models reconstructed after micro-computed tomography, (b) morphometry of smooth muscles/connective tissue ratio, collagen type I/III ratio, and area of TGF-beta-1 expression in corpora cavernosa, and (c) RT-PCR of TGF-beta-1 expression.

Results: Micro-computed tomography allowed visualization of penile structures at a resolution comparable to light microscopy. Gray values of corpora cavernosa decreased from 1673 (1512–1773) on the initial day to 1184 (1089–1232) on the 21st day ($p < 0.005$). However, on the 84th day, it increased to 1610 (1551–1768). On 21st and 84th days, there was observed a significant decrease in smooth muscle/connective tissue ratio and a significant increase in collagen type I/III ratio ($p < 0.05$). TGF-beta1 expression increased on the 84th day according to immunohistochemistry ($p < 0.005$). RT-PCR was impossible to conduct due to the absence of RNA in obtained samples after micro-CT.

Discussion and conclusions: Micro-computed tomography provided 3D visualization of entire corpora cavernosa and assessment of radiodensity alterations by gray value

Funding information
Foundation for Assistance to Small Innovative Enterprises in Science and Technology, Grant/Award Number: 15849ГУ/2020; Ministry of Science and Higher Education of the Russian Federation, Grant/Award Number: BAZ 0110/20-5-14AB; Megagrants, Grant/Award Number: 14.Z50.31.0046

analysis in fibrosis progression. We speculate that gray value changes at early and late fibrosis stages could be related to tissue reorganization. RT-PCR is impossible to conduct on tissue samples studied by micro-CT due to RNA destruction. We also suggest that micro-computed tomography could negatively affect the immunohistochemical outcome, as a significant increase of TGF-beta-1 expression occurs later than histological fibrotic signs.

KEYWORDS
3D X-ray microscopy, animal model, cavernous fibrosis, corpora cavernosa, gray value analysis, micro-computed tomography, penis, radiodensity

1 | INTRODUCTION

Penile cavernous fibrosis (CF) is an important pathologic condition leading to erectile dysfunction. It represents structural alterations of the corpus cavernosum tissues, such as loss of smooth muscle cells by apoptosis and transformation of fibroblasts into the myofibroblasts, producing extracellular matrix proteins.[1]

Understanding the processes of penile fibrogenesis is essential for physicians because the management of erectile dysfunction depends on the severity of penile morphological changes. While in mild stages, non-invasive treatment could be effective, whereas only surgical treatment is required in complicated cases.[2] In clinical practice, ultrasonography and computed tomography could be used to evaluate the cavernous septum' condition of patients who do not respond to orally active agents.[3,4]

Imaging, especially non-destructive, is needed in pre-clinical trials. In these studies, rat models are usually used, which are based on four major conditions associated with CF: testosterone deficiency, aging, diabetes mellitus, and cavernous nerves injury.[5] The only available method of penile visualization in rats is the histopathological analysis due to the relatively small penis size of the laboratory animals. Also, the time intervals of taking penile samples for these purposes vary depending on the CF model because of different dynamics of fibrogenesis caused by pathology in NO-cGMP, TGF-β, SHH, VEGF, and ROCK signaling pathways.[6] For instance, while CF occurs rapidly following cavernous nerve injury and castration within 2–4 weeks,[7,8] in diabetes mellitus, similar morphological changes can be observed within 6–12 weeks,[9,10] and in aging signs of CF could be detected throughout the entire life of laboratory animals.[11]

One of the perspective diagnostic methods for CF is micro-computed tomography (micro-CT). It provides the complex 3D visualization of fibrotic processes in various organs of laboratory animals.[12,13] Moreover, micro-CT enables tissue radiodensity assessment by gray value analysis, where high values indicate higher density and low values – lower density similar to Hounsfield scale.[14,15] However, this method has rarely been used for morphological analysis of soft penile tissue in animal models. In this study, we assessed the dynamic of penile fibrogenesis and gray value changes of corpora cavernosa by micro-CT in a rabbit model of CF and made a comparison with (a) histological analysis by hematoxylin and eosin (H&E) and Masson trichrome staining, (b) histochemical analysis by Sirius red staining, (c) immunohistochemical analysis of TGF-beta-1 expression, and (d) performed real-time PCR with reverse transcription for TGF-beta-1 expression evaluation in penile tissue samples.

2 | MATERIALS AND METHODS

2.1 | Animals, surgical procedure, and study design

Twenty-five male 23.5 ± 0.8 weeks old white New Zealand rabbits were obtained from Don State Technical University. All animals underwent bilateral orchidectomy on the initial day of the experiment and then were randomly divided into four groups based on the day of performing penectomy with urethral reconstruction: initial/0th day ($n = 5$), 7th day ($n = 5$), 14th day ($n = 5$), 21st day ($n = 5$), and 84th day ($n = 5$). All samples of penile tissues were fixed in 10% neutral buffered formalin. Blood samples were taken from every animal before any interventions and on the 7th, 14th, and 21st day for measuring serum total testosterone level by chemiluminescent microparticle immunoassay (Abbott ARCHITECT i2000, Abbott Park, IL, USA). After conducting experiments, all animals were kept under healthcare control for 1 month. No lethal cases were registered.

2.2 | Sample preparation and staining

After initial fixation in 10% formalin for 48 h, all penile samples were gradually dehydrated in 50, 70, 80, 90, 96, and 100% ethanol for 1 h in each solution. Then samples were stained in 1% wt I_2 solution in absolute ethanol for 14 h. Finally, samples were washed in absolute ethanol and subsequently placed in plastic containers filled with absolute ethanol and stored at 5°C.[16]

2.3 | Image acquisition and processing

Micro-CT research was conducted using the Xradia Versa 520 unit (Carl Zeiss X-ray Microscopy Inc., Pleasanton, CA, USA). All the

samples were placed on the holders inside plastic tubes filled with absolute ethanol. Acquisition parameters were identical for all the samples: magnification objective, 0.4x; voltage, 60 kV; power, 4.5 W; source filter, LE3; exposure time, 1.5 s; and voxel size, 50 μm. For each sample, 1601 X-ray projections were acquired, which were afterward reconstructed using XRMReconstructor 12.0.8086.19558 software (Carl Zeiss AG, Jena, Germany) with automatically adjusted center shift values, $\sigma = 0.5$ Gauss blurring filter and standard beam hardening correction ratio of 0.05. The correction of sample drift was enabled.

For each scan, the sample was placed at the closest possible distance to the X-ray source for the whole sample to be imaged. A2048 × 2048 pixels CCD camera was maintained at −59°C. The acquisition was performed with a camera binning factor = 2, which resulted in up to 1024 × 1024 pixels-sized projection images. The X-ray source filter was selected based on the observed transmittance values according to the recommendations of the Xradia Versa 520 manufacturer. The exposure time was selected to maintain count (intensity) values greater than 5000 with the selected source parameters and filter. The dynamic ring removal option, which enables small random motions of the sample during acquisition, was enabled for each sample's projections. Twenty-five reference X-ray images were acquired during each tomography procedure with equal time intervals between them (the air was used as reference). The average of these references was applied to each projection. Before each acquisition, up to 1 h warm-up scan was performed with the same source parameters.

2.4 | Volume rendering and measurements

After data acquisition, the images were exported in DICOM format for volume rendering in VGSTUDIO MAX 3.4 software (Volume Graphics GmbH, Heidelberg, Germany). The imported DICOM files were rendered by the volume renderer (Scatter HQ) algorithm. A semi-automatic region growing instrument was used to provide segmentation of the regions of interest (ROI) - corpora cavernosa. Gray value analysis was performed to research the radiodensity of the tissue inside the ROI in terms of mean gray value (MGV).

2.5 | Histopathologic analysis

After micro-CT imaging, samples were cut in the projection of ROI corresponding to micro-CT data and embedded in paraffin for further staining with H&E and Masson's trichrome. The slices obtained from the paraffin blocks were scanned using a histological slide scanner Aperio AT2 (Leica, Wetzlar, Germany). Histopathological slides stained by Masson's trichrome stain were used for morphometry. Corpora cavernosa were discerned as ROI.

2.6 | Histochemical analysis

For histochemistry and collagen type I and III detection, serial paraffin sections were stained with Sirius red 21–040 kit (Biovitrum, St. Petersburg, Russia) and were visualized in a polarizing Leica DM6000 B microscope (Leica, Wetzlar, Germany) with Leica DFC500 camera (Leica) and Leica Application Suite 4.6 program (Leica Microsystems, Heerbrugg, Switzerland).

2.7 | Immunohistochemical analysis

For the immunohistochemical study, a primary rabbit polyclonal antibody against TGF-beta-1 in dilution 1:100 was used (Cloud-Clone Corp., Houston, USA). The Dako Envision System + Peroxidase detection system (Daco, Glostrup, Denmark) was used to visualize antigenic activity. The immunohistochemical reaction was followed by hematoxylin counterstaining. Obtained slides were scanned using a histological slide scanner Aperio AT2 (Leica). For a detailed examination of antigenic activity, Leica DM2500 microscope (Leica) with Leica DFC 495 camera (Leica) and Leica Application Suite 4.6 program (Leica Microsystems, Heerbrugg, Switzerland) were used.

2.8 | TGF-beta-1 expression study using real-time PCR with reverse transcription

The innuPREP FFPE Total RNA Kit (Analytik Jena AG, Jena, Germany) was used to isolate RNA from FFPE samples, and the kit protocol was followed. The isolated RNA was then treated with DNase I (Thermo Fisher Scientific, Waltham, USA) according to the supplied protocol. Complementary DNA (cDNA) was obtained using the «OT-1» reverse transcription kit (Syntol, Moscow, Russia) using the following protocol: 40 min at 40°C and 8 min at 92°C. The mix composition was in agreement with the «OT-1» kit protocol. RT-PCR was performed using the GAPDH as a reference gene and the original primers, developed with Primer3 and protocol (Table 1). RT-PCR was performed in QuantStudio 5 Real-Time PCR System (Thermo Fisher Scientific) using VeriFlex temperature control technology to provide annealing of primers with different melting temperatures. The total concentration of RNA in the samples was additionally measured by spectrophotometry using a NanoPhotometer P 330 (Implen, München, Germany).

2.9 | Morphometric analysis, statistics, and ethics

Obtained histopathological images were analyzed using QuPath open-source software.[17] We performed the morphometrical analysis of (a) smooth muscle/connective tissue ratio (SM/CT) based on the engaged area percentage of selected ROI components by assigning corresponding thresholds to each color (collagen fibers were stained as blue and

TABLE 1 Primers and protocol for RT-PCR to study TGF-beta-1 gene expression

Primers			
Gene	**Temperature (°C)**	**Forward**	**Reverse**
TGF-beta-1	58.8	5′-ACGGAGAGGAAATAGAGGGC-3′	5′-TGTGTAGATGTTGAGCCCGT-3′
GAPDH	59.2	5′-CATGTTTGTGATGGGCGTGA-3′	5′-GGAGGCAGGGATGATGTTCT-3′
Protocol conditions			
Step	**Time (s)**	**Temperature (°C)**	**Cycles**
Initial denaturation	300	95	1
Denaturation	20	94	40
Annealing	30	58.8/59.2	-
Extension	40	72	-

smooth muscle cells as red by Masson's trichrome stain), (b) collagen type I/III (collagen I/III) ratio by calculation of red to light-green polarizing light ratio, and (c) TGF-beta-1 expression as a percentage of the covered area of corpora cavernosa (ROI) by the color display of antigenic activity.

GraphPad Prism v.8.4.2 (GraphPad Software, California, USA) was used for data analysis. All data were not normally distributed according to the Shapiro–Wilk test. For the data analysis, the Friedman test was used for related samples and the Kruskal-Wallis test for independent samples, followed by the Dunn-Bonferroni post hoc test. Spearman's correlation coefficient was used to examine the relationship between morphometric results and micro-CT gray value analysis of radiodensity. Results were presented as median and interquartile range. The statistical significance was determined as $p < 0.05$. All animal studies were carried out under the "Guide for the Care and Use of Laboratory Animals" and were approved by the ethics committee of the Don State Technical University, Rostov-on-Don, Russia (protocol number 67-43-1).

3 | RESULTS

3.1 | Total testosterone level

Mean serum total testosterone level of all animals before experiments were 8.64 (8.32–8.93) ng/ml and after 7 days from bilateral orchidectomy, it significantly decreased to 0.20 (0.15–0.29; $p < 0.0001$) and remained at a minimum level during the 14th day (0.18 (0.15–0.24) ng/ml; $p < 0.0001$) and 21st day (0.15 (0.15–0.20) ng/ml; $p < 0.0001$), indicating successful recreation of testosterone deficiency (Figure 1A).

3.2 | Visualization of penile structures

Twenty-five 3D models of rabbit penises were reconstructed based on micro-CT data. Two sagittal and three transversal slides per penile sample corresponding to 3D reconstructions were made. Sagittal and transversal sections of 3D models were made with correspondence to histological images. Basic penile structures such as corpora cavernosa, intracavernous pillars, and urethra are visualized both by histological and micro-CT imaging. However, 3D reconstructions with specified acquisition parameters do not provide visualization of cellular structures such as smooth muscle cells of corpora cavernosa and endothelium of penile vessels, which are perfectly visible on histological slides stained by H&E. Nonetheless, micro-CT enabled comprehensive visualization of surface and inner structures at the same and for the entire length of penises (Figure 2).

3.3 | Mean gray value analysis

Corpora cavernosa of each reconstructed 3D penile model were highlighted as ROI following gray value analysis. The "plasma" perceptually uniform color scheme was used to visualize the radiodensity alterations (Figure 3). According to the gray value analysis, the MGV of the initial day group of animals is 1673 (1512–1773), and this index became significantly lower in animals after 21 (1184 (1089–1232); $p < 0.0001$) days of induced testosterone deficiency. However, radiodensity assessed by gray value analysis increased significantly on the 84th day to 1610 (1551–1768) MGV relative on the 21st day (Figure 1B).

3.4 | Penile fibrosis assessment by Masson's trichrome staining analysis

Smooth muscles are present within intracavernous pillars and sinusoidal tissue in rabbits of the initial day group, while in other groups, it visually decreased and is replaced by connective tissue. In 14- and 21-day samples, collagen fibers are strongly present in the intercellular space of sinusoidal tissue. After 84 days from orchidectomy, smooth muscles are poorly presented in corpora cavernosa and almost completely replaced by connective tissue indicating total CF (Figure 4). The accumulation of collagen in corpora cavernosa is also seen with a significant SM/CT ratio decrease on the 21st and 84th days after testosterone deprivation ($p < 0.0001$; Figure 1C).

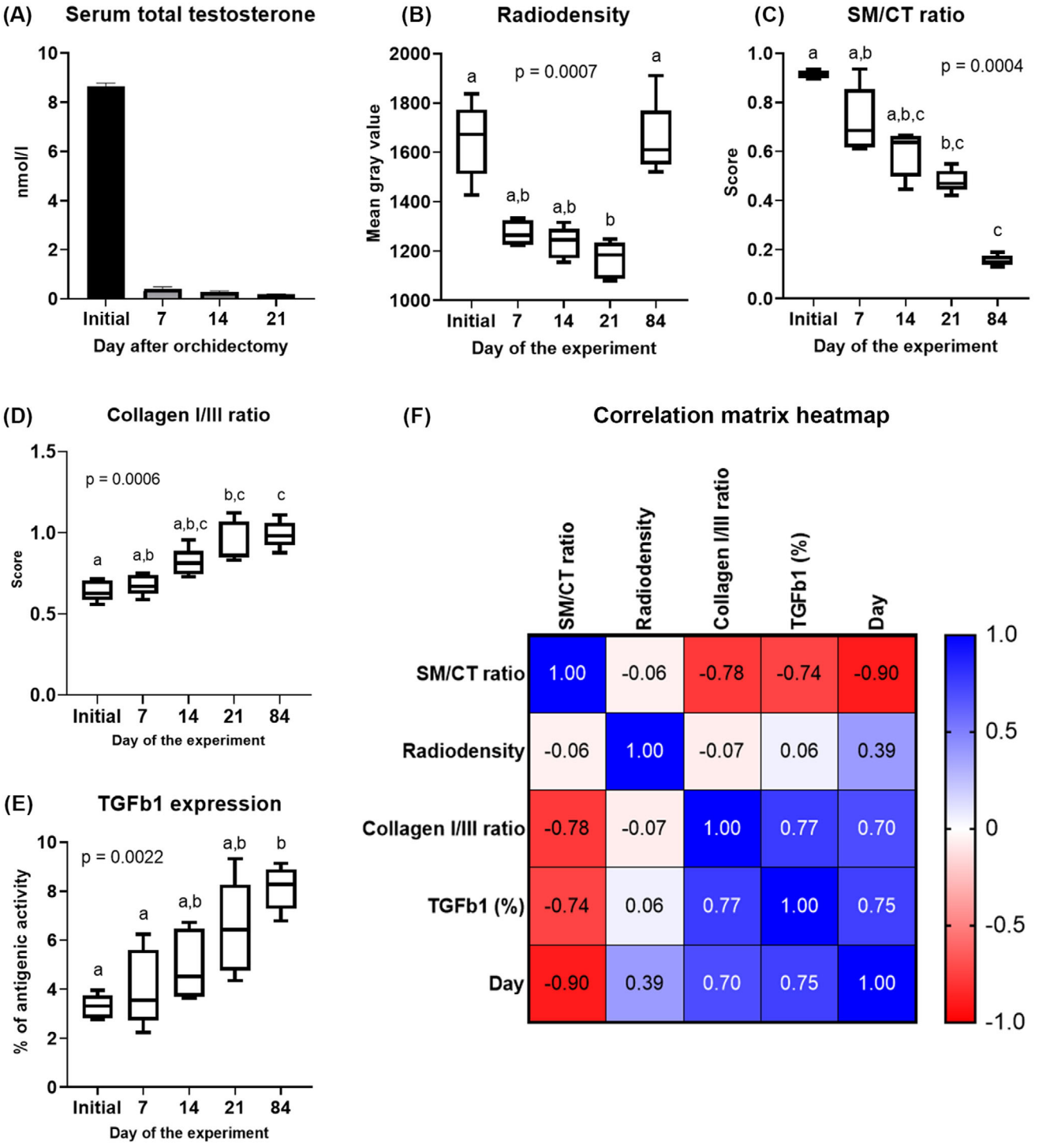

FIGURE 1 Statistical outcomes: (A) serum total testosterone changes, (B) changes of radiodensity by gray value analysis of corpora cavernosa, (C) changes of smooth muscle/connective tissue (SM/CT) ratio in corpora cavernosa during the experiment, (D) changes of type I/III collagen (collagen I/III) ratio in corpora cavernosa during the experiment, (E) changes of immunohistochemical TGF-beta-1 (TGFb1) expression in corpora cavernosa during the experiment, and (D) the correlation between morphometric data and micro-computed tomography gray value analysis. Provided *p*-values are results of (A) the Friedman test and (B–E) the Kruskal-Wallis test, followed by the Dunn-Bonferroni post hoc test. Means within the same row without common superscripts are significantly different ($p < 0.05$)

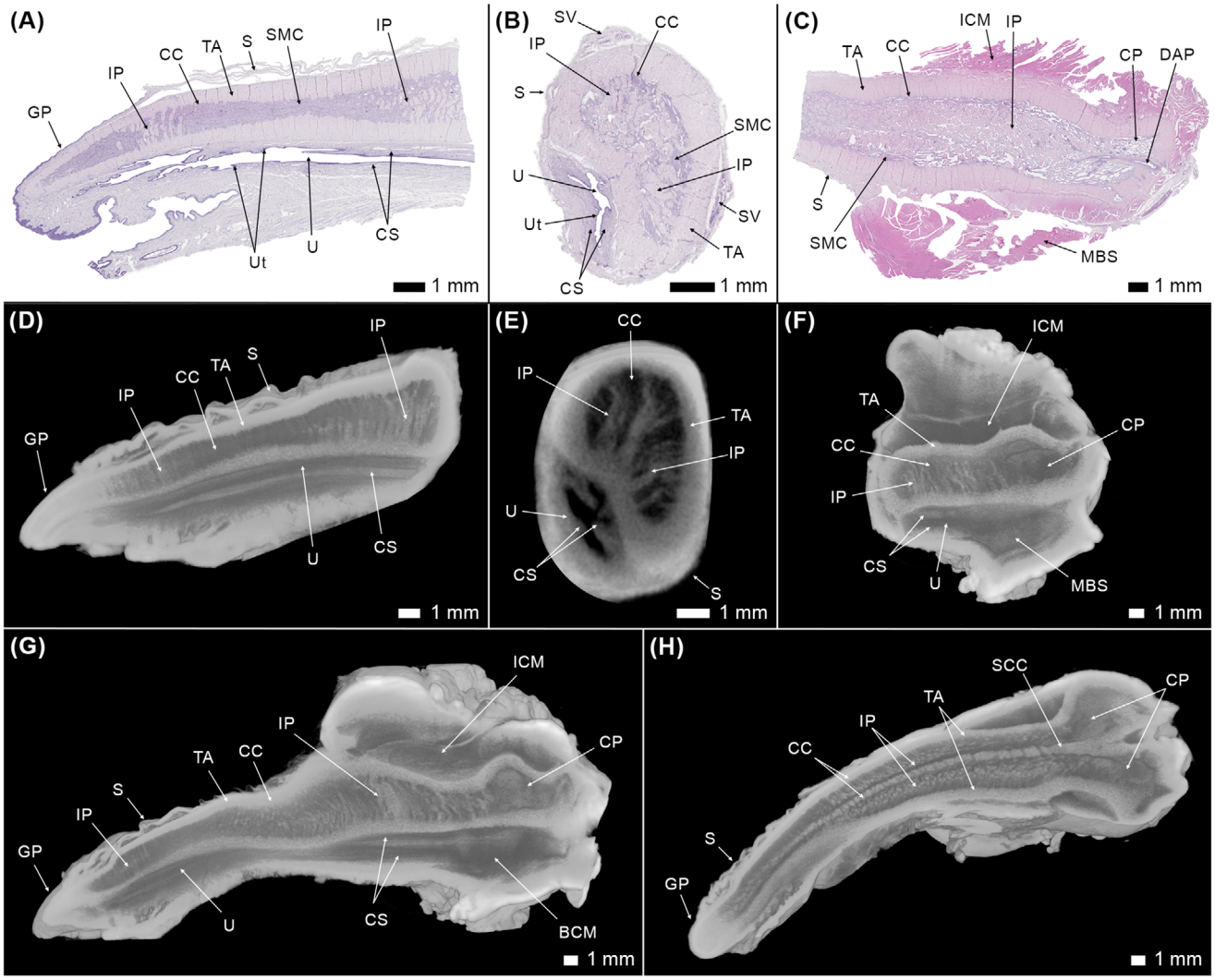

FIGURE 2 Comparison of histopathological and micro-computed tomography imaging of a typical rabbit penis: (A) sagittal-apical, (B) transversal-middle and (C) sagittal-basal histopathological slides, corresponding to their (D–F) micro-computed tomography sections, (G) sagittal, and (H) frontal sections of a full-size penile 3D model. S, skin; ICM, ischiocavernosus muscle; CP, crus penis; GP, glans penis; TA, tunica albuginea; CC, corpus cavernosum; SV, superficial veins; DAP, deep arteria of the penis; SCC, septum of corpora cavernosa; IP, intracavernous pillars; CS, corpus spongiosum; U, urethra; Ut, urothelium

3.5 | Collagen I/III ratio

Histochemical Sirius red staining allowed types I and III collagen to be visualized at the corresponding histological slides by red and light-green polarizing light, respectively. Types I and III collagen are represented in all obtained samples. In samples obtained before orchidectomy, type I collagen is poorly presented in intracavernous pillars and sinusoidal tissue of corpora cavernosa, relatively to type III. However, type I collagen visually prevails in CF progression, reaching the most prominent presence on the 21st and 84th days. Also, the severity of polarization visually increases throughout testosterone recreation at each time point (Figure 5). According to morphometric analysis collagen I/III, the ratio increases significantly on 21st and 84th days after orchidectomy ($p < 0.05$; Figure 1D).

3.6 | TGF-beta-1 expression by immunohistochemistry

On all obtained samples, the antigenic reaction against TGF-beta-1 allows differing smooth muscles and connective tissue due to the relatively high expression of TGF-beta-1 in the connective tissue of corpora cavernosa. On the 14th, 21st, and 84th days, the membrane staining of smooth muscle cells in the form of a ring and diffuse dispersed staining of the intercellular space is observed. Simultaneously, the severity of TGF-beta-1 expression increases with the duration of the experiment. On the 84th day, intercellular expression of TGF-beta-1 reaches its peak relative to samples obtained at other time points of the experiment (Figure 6). The morphometric analysis allowed the calculation of color representation of antigenic activity against TGF-beta-1 as a

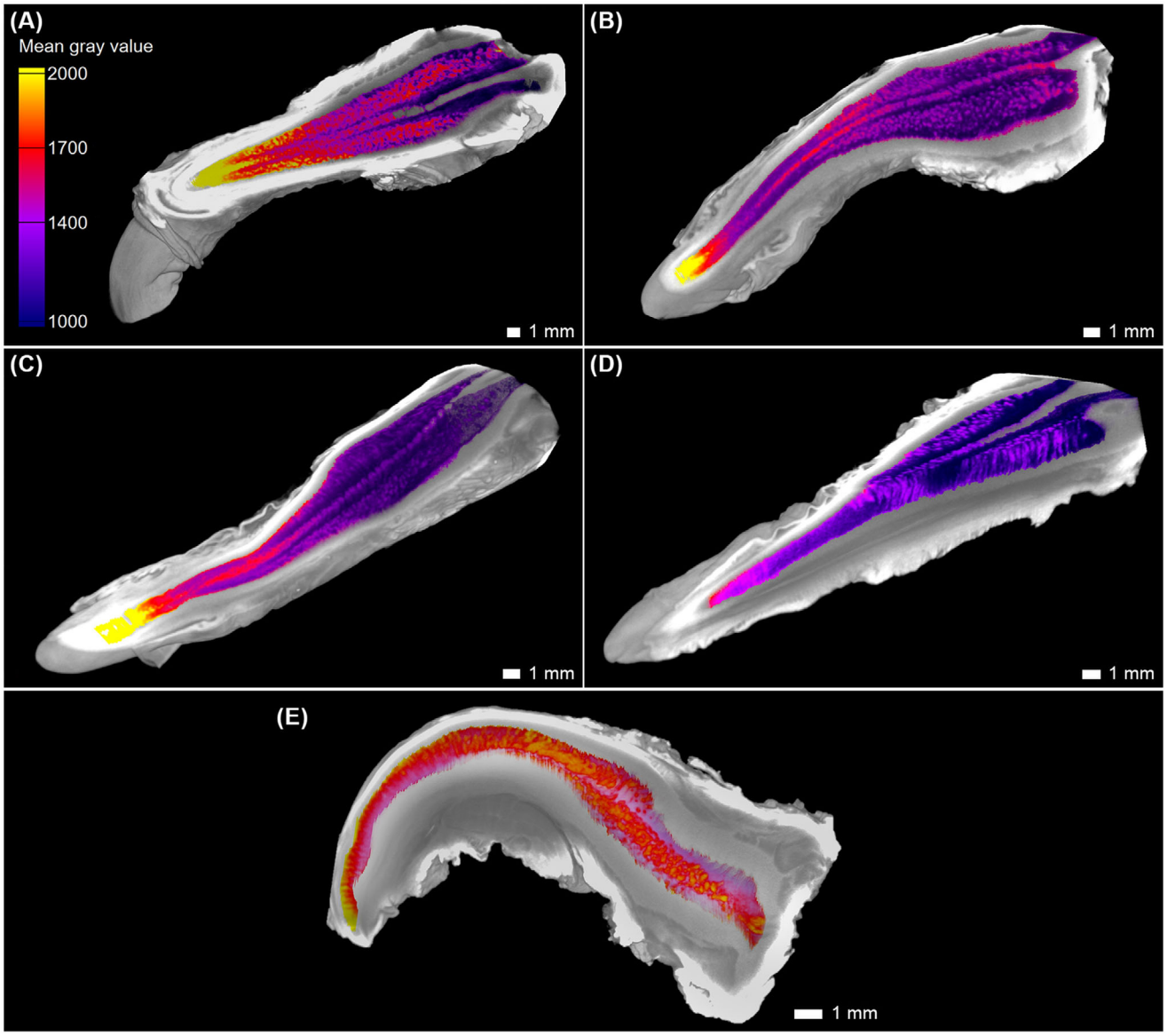

FIGURE 3 Visualization of dynamical occurrence of gray value changes by "plasma" uniform scheme in corpora cavernosa of laboratory rabbits with reproduced testosterone deficiency: (A) initially, (B) 7th day, (C) 14th day, 21st day, and (E) 84th day. Higher gray values indicate higher radiodensity and lower gray values indicate lower radiodensity

percentage of the covered area of corpora cavernosa. Throughout the experiment, the TGF-beta-1 expression rises gradually, but significant changes were observed only after 84 days from orchidectomy (Figure 1E).

3.7 | TGF-beta-1 expression by RT-PCR

RT-PCR did not determine the pattern of change in TGF-beta-1 expression due to the presence of DNA in the RT-negative control samples, which were treated by DNase and not included in the reverse transcription reaction. The initial hypothesis of failed RT-PCR was based on insufficient DNase activity, but this result was repeated after using a new reagent. The RNA content before DNase treatment was also measured in control tissue samples that have not undergone micro-CT (rabbit kidney and lymph nodes) and in samples that have undergone micro-CT. It was found that RNA content in the control samples ranged from 16.4 to 42 ng/μl, while RNA content in the samples after micro-CT was 3.6 ng/μl or lower, with only one sample showing an RNA content of 10 ng/μl.

3.8 | Correlation heatmap analysis

A significant negative correlation was shown for SM/CT ratio and collagen I/III ratio, TGF-beta-1 expression in corpora cavernosa, and day of the experiment (p-value < 0.0001). At the same time, a significant positive correlation is shown for TGFb expression in corpora cavernosa and

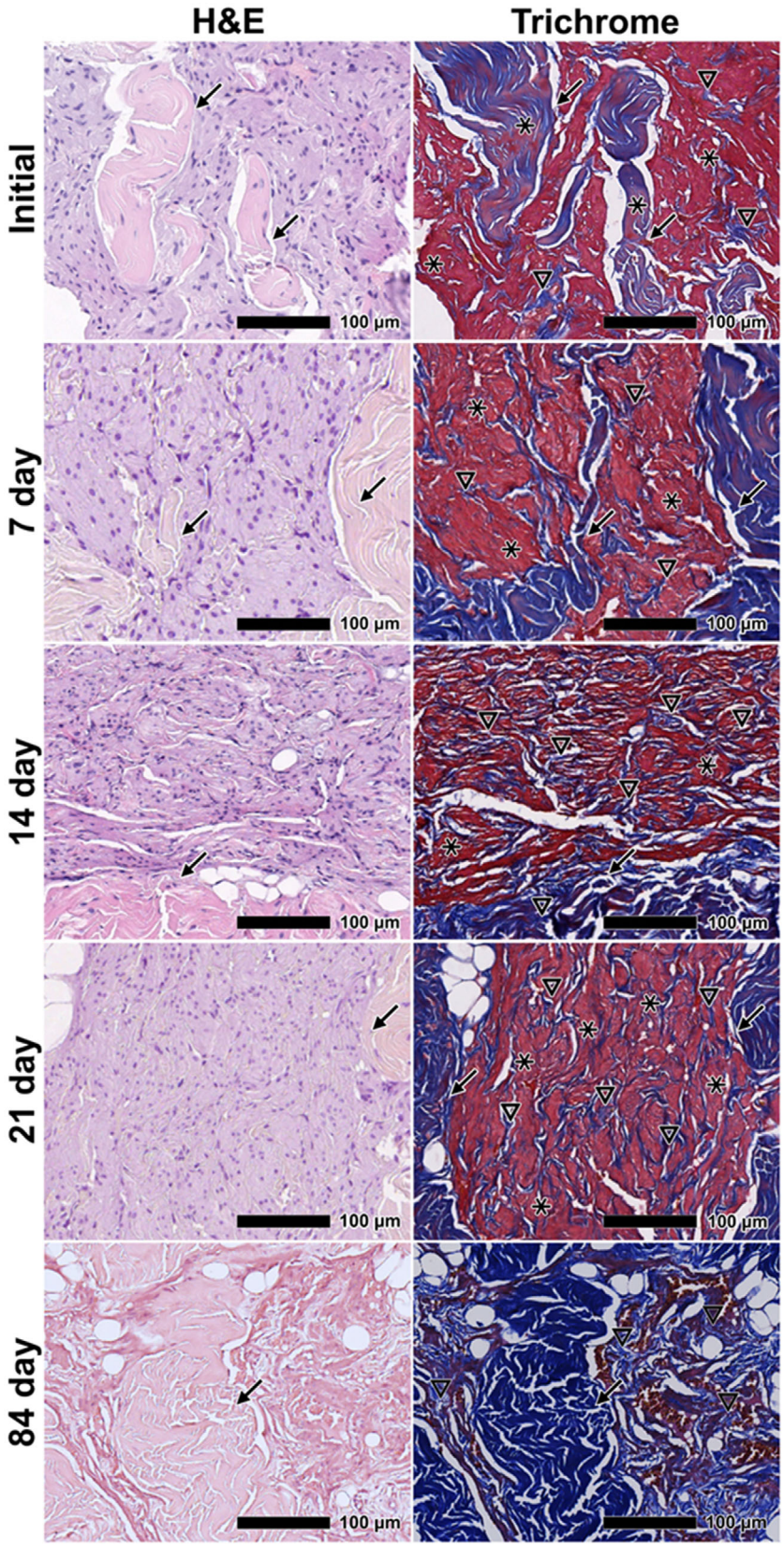

FIGURE 4 Representative images of hematoxylin and eosin (H&E) and Masson's trichrome staining of penile corpora cavernosa on different experiment days (scale bars provided for each image). In samples of corpora cavernosa, obtained before testosterone deprivation, the connective tissue (stained as blue by Masson's staining) is located in intracavernosal pillars and poorly presented in the intercellular space of smooth muscles (stained as red by Masson's staining). In 7, 14, 21, and 84 days, the spread of connective tissue in intercellular space increases at each time point, reaching its peak in 84 days. The spread of connective tissue is chaotic at the early stages of cavernosal fibrosis. In contrast, it is orderly distributed in the almost complete absence of smooth muscles at the later stage. Trabecular smooth muscle cells are represented by asterisks, collagen fibers by triangles, and intracavernous pillars by arrows. Microphotographs are obtained by a histological slide scanner

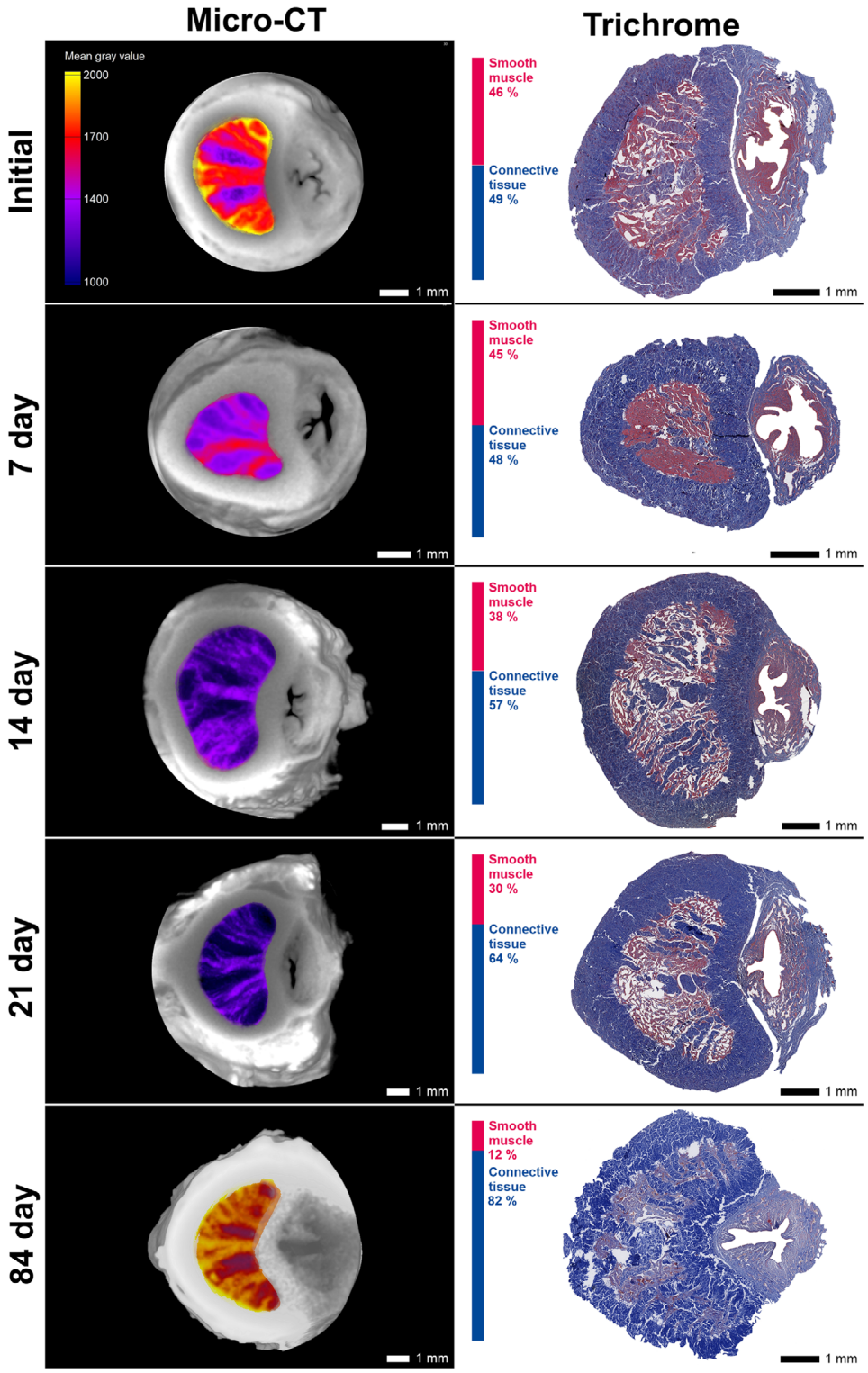

FIGURE 5 Representative figures of transversal sections of 3D penile models and Masson's trichrome-stained histological slides of corpora cavernosa corresponding to each other. Radiodensity decreases from the initial day of the experiment up to 21 days, followed by decreasing smooth muscle and increasing connective tissue presence in corpora cavernosa. However, in 84 days, radiodensity is increased and mean gray values are comparable to those of samples obtained on the initial day of the experiment. At the same time presence of smooth muscles after 84 days from castration remains at a minimum. An increase in radiodensity could be related to tissue reorganization. While in the early stages (7, 14, and 21 days) of cavernous fibrosis, the spreading of connective tissue is chaotic, in the late stage (84 days), the directions and presence of the connective tissue fibers are ordered, which is better seen at greater magnification

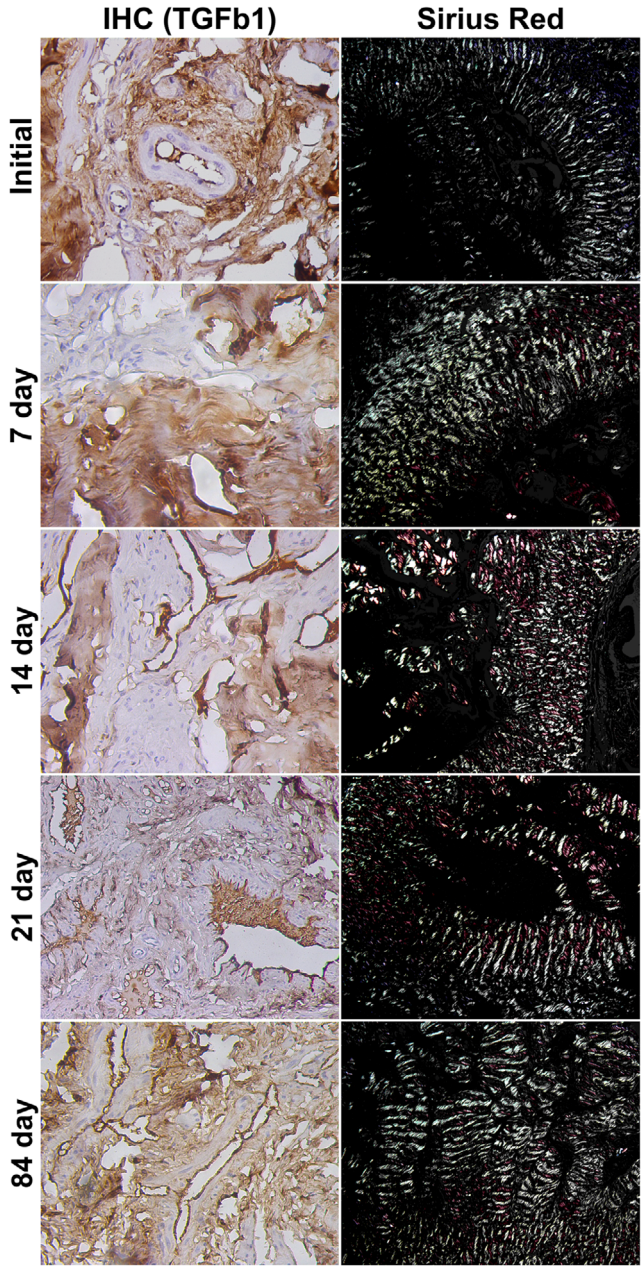

FIGURE 6 Results of immunohistochemical (IHC) analysis for TGF-beta-1 (TGFb1) expression (400xmagnification) and Sirius red staining for analysis of type I (stained as red) and III (stained as light green) collagen presence (50x magnification) in corpora cavernosa. There is visualized the gradual increase of TGF-beta-1expression from 7 to 84 days of the experiment. The samples are characterized by high antigenic activity in the form of colored brown staining. On the 84th day, the expression of TGF-beta-1 in the intercellular space of smooth muscles is highly mostly presented, as well as the expression of type I collagen in corpora cavernosa compared to the samples obtained before orchidectomy. Microphotographs are obtained by microscopes with cameras

collagen I/III ratio with the day of the experiment (p-value < 0.00001). As shown in Figure 1, SM/CT ratio decreases gradually throughout the experiment, with the simultaneous increase of collagen I/III ratio, TGF-beta-1 expression, which indicates the relationship of all of these parameters. However, the increase of radiodensity of corpora cavernosa after 84 days is not associated with any studied parameter.

4 | DISCUSSION

In this study, we assessed CF by micro-CT, histological, histochemical, and RT-PCR methods and compared the visualization capabilities of histological and micro-CT imaging of penile tissue. We chose a rabbit model over other laboratory animals because of the relatively bigger size of the penis and the absence of a baculum. In most previous studies, micro-CT of penises was used on animals known for the presence of baculum. These studies' main aim was to examine surface and internal morphological features of penile bone obtained from healthy animals.[18,19] However, there is a lack of micro-CT visualization data of soft penile tissues and especially the ability to follow their alterations.

The only paper in this area we found was published by Simopoulos et al. almost 20 years ago.[20] In that study, rabbits were used in an alloxan-induced diabetes mellitus model, and identical morphological alterations in corpora cavernosa occurred due to the same action of hyperglycemia and testosterone deficiency on NO-cGMP, TGF-β1, VEGF, SHH, and ROCK signaling pathways.[21] Although the intensity of trabecular smooth muscle replacement with connective tissue varies. In severely diabetic rabbits, the decrease in the mean percent of smooth muscle is reported to the range from 42.4 ± 1.5 to 35.8 ± 1.5% after 6 weeks from alloxan treatment,[20] while almost the same percent is observed in rabbits after 2 weeks from bilateral orchiectomy decrease, namely from 45% (43.5–45%) to 37% (30.5–37.5%) and from 0.92 (0.89–0.93) to 0.64 (0.49–0.66) SM/CT ratio, respectively. However, in our work, significant changes calculated with adjusted criteria are seen only in 21 days with 31% (28.5–33%) smooth muscle prevalence and 0.47 (0.44–0.52%) SM/CT ratio, for what is considered as severe CF, and in 84 days with 12% (11.5–14%) smooth muscle prevalence and 0.15 (0.13–0.18) SM/CT ratio, for what is considered as total CF (Figures 1C and 4).

Although volume-rendered 3D models of rabbit penises generated in Simopoulos et al. study are anatomically similar to ours, the sample preparation and X-ray micro-CT scanning are different. In the previous study, penile perfusion was performed by vasodilator drugs and followed by radiopaque silicone rubber. This technique provided better vascular structures visualization as they are dilated due to the injection of filling silicone rubber and allowed estimation of the volume decrease of cavernous arteries and sinusoidal space in diabetic rabbits. In our study, iodine staining was used for penile tissue contrast, allowing for the better visualization of inner structures by micro-CT. We chose iodine over osmium tetroxide as it does not require special equipment to work with and does not pose a danger to laboratory personnel.[22] Furthermore, it is previously described that iodine staining is

compatible with following H&E and Masson's trichrome histopathological staining, in contrast to phosphotungstic acid staining.[23]

For a better understanding of using micro-CT in the assessment of CF, we also studied collagen I/II ratio and TGF-beta-1 expression by immunohistochemistry and RT-PCR in penile samples that underwent micro-CT. The collagen in the corpus cavernosum tissue is predominantly types I, III, and IV.[24] Alteration of collagen I/III ratio in corpora cavernosa, which could be visualized by Sirius red staining, is often described as part of CF alterations. Ren et al. described the significant increase of type I collagen deposition with its following prevalence over type III collagen in rabbits with penile fibrotic alteration compared to the control group.[25] De Souza et al. also reported that in rats I collagen significantly rose with increasing connective tissue presence visualized by Masson's trichrome stain after reproduction of CF by chronic stress.[26] Increase of type I collagen throughout CF progression could be related to tissue remodeling. Type III collagen is present in elastic distensible tissue, such as penile corpora cavernosa and tunica albuginea. Tissue distensibility is essential for the veno-occlusive mechanism, as it needs normal tensile tissue strength to act.[27,28] On the other hand, type I collagen is known for stiff bands of connective tissue fibrils. Its extensive deposition and prevalence over type III collagen leads to a loss of penile elasticity and, as a result, erectile dysfunction.[27–29] Our study also shows that the severity of CF confirmed by the replacement of smooth muscles with connective tissue has a significant correlation with excessive deposition of type I collagen over type III collagen (Figure 1F).

We chose TGF-beta-1 expression for CF assessment, as this pleiotropic cytokine has been shown to induce collagen synthesis in cavernosal tissue in vitro.[30,31] Also, TGF-beta-1 overexpression is associated with CF occurrence in animal and human studies, making it one of the CF markers.[9,32,33] Unfortunately, it was technically impossible to conduct RT-PCR to analyze TGF-beta-1 expression due to the absence of RNA in penile tissue samples that underwent micro-CT. RNA disruption during micro-CT was the reason why TGF-beta-1 expression analysis could not be performed and also provoked low efficiency of DNase processing, probably due to the formation of crosslinks in the DNA, making it inaccessible to DNase.[34] The study's main aim was to compare the capabilities of micro-CT imaging and radiodensity assessment for CF evaluation in the whole penile sample with the following analysis by acknowledged methods, such as histological, histochemical, immunohistochemical, and RT-PCR evaluation. It seems that micro-CT itself affects studied tissues altering following results by other evaluation methods. According to our subjective view, additional iodine-ethanol staining could result in harder sample preparation for the histological, histochemical, and immunohistochemical assessment. First, tissues became slightly harder for microtome cutting, probably because of additional dehydration for micro-CT staining. We are sure that this did not alter the morphometrical outcome obtained from Masson's trichrome and Sirius red-stained slides, but it brought more artifacts in histological view. Also, additional time for iodine-ethanol staining for micro-CT could alter the results of the immunohistochemical analysis. The overall time for iodine-ethanol staining and micro-CT procedure for tissue samples from each group in our study was to 3 days. Webster et al. reported a negative relationship between tissues immunoreactivity and prolongation of their fixation. They showed that the brightness of color representation of antigenic activity decreases over fixation time.[35] That is why we believe that prolonged fixation in ethanol could alter the morphometrical outcome of TGF-beta-1 expression, as other researchers report its significant increase at early stages of CF at the same time as other fibrosis signs,[36] while in our study, significant changes are observed at the late stages of CF (Figure 1E). We think that the best way to avoid these problems is to use different tissue parts of the penis for different analyzing methods. In our opinion, the ability to obtain quantitative data for statistical analysis is a priority in animal studies and pre-clinical trials than complete 3D visualization of the penis on micro-CT, which would be impossible when scanning a part of the penis. Our research allowed us to identify these problems in order to avoid them in further penile micro-CT studies.

The most significant outcome of our study is radiodensity changes in CF progression. For the quantitative micro-CT radiodensity assessment throughout CF progression, we used an analysis of gray value – level of brightness of a pixel or voxel.[37,38] Previous studies showed a significant relationship between tissue density and MGV, indicating gray value analysis as a method for indirect tissue density assessment.[38,39] In our study, at the early stages of CF, MGV is decreased compared to the initial stage, while at the late stage, it is increased (Figures 1D, 3, and 5). Because of this, no significant correlation with other parameters is observed (Figure 1F). We speculate the reason for this is the progressive disorganization of normal penile histological architecture with smooth muscle replacement by chaotic and excessive accumulation of collagen fibers at the early stage and connective tissue organization similar to scarring at the late stage. As it is shown in Figure 4, the direction of connective tissue fibers differs depending on the CF stage, while at the early stage (7, 14, and 21 days), it is chaotic (connective tissue fibers spreads among intercellular space of smooth muscle), at the late stage (84 days), it is orderly distributed primarily because of nearly total replacement of smooth muscles by connective tissue. This hypothesis needs further studies to be proven. At the moment, thisis just a subjective view on radiodensity changes at the late fibrosis stage based on the description of histological slides. However, there is a clear trend of radiodensity decrease at the early stages of CF, reaching its significance on the 21st day (Figure 1B). Therefore, we believe that radiodensity obtained from micro-CT could be used as an additional CF assessment parameter in animal studies and pre-clinical trials for investigating new ways of topical or local CF prevention and treatment, such as extracorporeal shockwave therapy or intracorporeal injection of stem cells.[40,41] If the treatment is effective, the radiodensity should not change and remain the same level as in control groups. This statement should obtain more evidence basement in further studies.

One of the study's limitations is micro-CT acquisition parameters, i.e., larger magnification and smaller voxel size could better visualize penile fibrotic alterations. For example, Tkachev et al. made a 3D reconstruction of the human's eye part that allowed differing superficial and basal epithelium of the cornea.[42] In this study, the magnification objective was 4x with voxel size 2.5 μm. While in our

work, acquisition parameters for corpora cavernosa were 0.4x for magnification objective and 50 μm for voxel size, resulting in relatively less detailed visualization. We believe that larger magnification and smaller voxel size can better visualize tissue remodeling during CF. At least we could be able to differentiate types of tissues according to MGV at transversal slides of 3D reconstructions of corpora cavernosa, as shown in the study by Tkachev et al.[42] Also, we suggest that nucleus-specific staining prior to micro-CT could enable appropriate 3D visualization of smooth muscle cells replacement in CF.[43] For direct penile density assessment, calibration phantoms with set density are needed.[39] Making such phantoms referred to soft penile tissue needs further biomechanical investigations.

Micro-CT is not the only method for 3D tissue visualization. The 3D pathohistological analysis procedures in development are based on the volume tissue reconstruction of sequentially ordered histological slides. However, apart from being destructive, it can also lead to deformation, displacement, and ruptures occurring during sample preparation that could generate artifacts. These inaccuracies, in turn, may compromise image registration for precise alignment and 3D histological reconstruction affecting the whole visualization process and accuracy of diagnosis.[44] Based on this, we find micro-CT a very convenient and stable 3D visualization method as it is less time-consuming and requires a relatively simple sample preparation protocol consisting of dehydration and staining. It also provides a basis for selective ROI analysis by the following histopathology.

This study creates a foundation for radiodensity investigation of the penile tissue with CF, which is directly related to erectile dysfunction. Unfortunately, at the moment, X-ray micro-CT cannot be used in human medicine for in vivo diagnosis as the size of the tissue samples is limited for entering the scanning chamber of a laboratory-based micro-CT system. Our study is focused on ex vivo evaluation of tissues' properties, as Xradia Versa 520 unit is not supposed for in vivo studies. There are micro-CT systems designed for rat and mice studies, which inquire contrast-enhanced 3D visualization structural changes of inner organs.[45–47] It should be noted that the capabilities of these systems for visualization in large magnification are several times lower than ex vivo micro-CT systems, which results in less detailed 3D reconstruction. However, these technical differences do not affect the ability to determine radiodensity.[48] That is why we are sure in vivo micro-CT can quantitatively assess the dynamics of CF radiodensity changes in one rat or mice multiple times at different time points.

We also believe that micro-CT could find its place in clinical andrological practice in the future, but several problems should be solved. First of all, it is necessary to create micro-CT with design features for scanning human penises. Furthermore, the design must include patient safety as rotating X-ray tubes and detectors can damage penile tissue. Also, it is necessary to study the effect of the multiple scanning by cone-beam X-ray micro-CT on the physiology of penile tissue in living animals before clinical use in patients. Most importantly, we should investigate in detail the causes and mechanism of changes in the radiodensity of the penis at different CF stages in order to know how to interpret this data in clinical practice.

However, we should note that micro-CT could be a less cost-effective method for 3D visualization than current routine approaches, such as magnetic resonance arteriography and computed tomography angiography of penile corpora cavernosa. So, first, they should be enhanced for wide use in clinical practice. But abovementioned methods are capable only for visualization and diagnosis of vascular alterations in corpora cavernosa, excluding the opportunity to obtain data of penile radiodensity.[4] The technical increase in the scanning resolution of clinical computed tomographs will make it possible to use detailed 3D visualization of the corpora cavernosa and determine radiodensity in clinical practice in the near future. At the same time, penile micro-CT could stay an ideal choice for 3D visualization and radiodensity assessment of penile corpora cavernosa in animal studies and pre-clinical trials of new methods of CF suppression.

5 | CONCLUSION

The observed features of micro-CT open new opportunities for urological and andrological animal studies and pre-clinical trials. It provides a complex visualization of the entire penile sample and qualitative and quantitative assessment of radiodensity in CF by gray value analysis. It is impossible to conduct RT-PCR on the tissue samples that underwent micro-CT because of RNA destruction during the cone-beam X-Ray scanning. The quality of the immunohistochemical analysis of tissue samples that underwent micro-CT is altered because of additional time for tissue fixation and staining for micro-CT. Radiodensity of corpora cavernosa decreases at the early stages of CF on a par with other CF signs – a decrease of SM/CT ratio and increase of collagen I/III ratio. But radiodensity increases at the late stage, which could be related to tissue reorganization. The causes and mechanism of changes in the corpora cavernosa radiodensity at different CF stages should be investigated in further studies. However, we are sure that radiodensity obtained from micro-CT could be used as an additional CF assessment parameter in animal studies and pre-clinical trials for investigating new ways of CF suppression.

ACKNOWLEDGMENTS

Igor V. Popov was supported by the grant of the Foundation for Assistance to Small Innovative Enterprises (Project no. 15849ГУ/2020). E. Y. Kirichenko and A. K. Logvinov were supported by the Ministry of Science and Higher Education of the Russian Federation (Project no. BAZ 0110/20-5-14AB). E. V. Sadyrin and B. I. Mitrin were supported by the Ministry of Science and Higher Education of the Russian Federation (Grant 14.Z50.31.0046). We thank Michael Chikindas and Michael Swain for editing assistance and Anton Osipenko, Vladimir Shitov, and Victor Mikhailishin for figures design assistance. Micro-CT was carried out in the Research and Education Center "Materials" of Don State Technical University (https://nano.donstu.ru/).

CONFLICT OF INTEREST

The authors declare to have no conflict of interest.

AUTHOR CONTRIBUTIONS

Igor V. Popov and Ilya V. Popov carried out animal experiments. Igor V. Popov, S. Yu. Tkachev, B. I. Mitrin, and E. V. Sadyrin carried out micro-computed tomography procedures and DICOM data analysis. D. G. Pasechnik, N. S. Karnaukhov, I. A. Sukhar, T. O. Lapteva, and A. Yu. Maksimov participated in the histopathological analysis. E. Y. Kirichenko, A. K. Logvinov, and M. A. Akimenko conducted the immunohistochemical and histochemical analysis. E. D. Kulaeva and E. Y. Kirichenko carried out RT-PCR. Igor V. Popov, E. D. Kulaeva, S. N. Kulba, D. G. Pasechnik, and A. M. Ermakov contributed to the morphometrical and statistical analysis and interpretation of data. Igor V. Popov, Ilya V. Popov, and S. Yu. Tkachev wrote the manuscript. E. Y. Kirichenko, A. M. Ermakov, and M. I. Kogan participated in the article screening, experiment design, and critically revising the manuscript. M. I. Kogan and Igor V. Popov conceived of this study and supervised the experiments and the manuscript drafting. All authors read and approved the final manuscript.

ORCID

Mikhail I. Kogan https://orcid.org/0000-0002-1710-0169
Igor V. Popov https://orcid.org/0000-0002-9223-8731
Boris I. Mitrin https://orcid.org/0000-0002-5639-274X
Evgeniy V. Sadyrin https://orcid.org/0000-0002-7770-1601
Ilya V. Popov https://orcid.org/0000-0002-4253-0435
Alexey M. Ermakov https://orcid.org/0000-0002-9834-3989

REFERENCES

1. Yafi FA, Jenkins L, Albersen M, et al. Erectile dysfunction. *Nat Rev Dis Prim*. 2016;2:16003.
2. Mobley DF, Khera M, Baum N. Recent advances in the treatment of erectile dysfunction. *Postgrad Med J*. 2017;93(1105):679-685.
3. Bertolotto M, Campo I, Sachs C, et al. Sonography of the penis/erectile dysfunction. *Abdom Radiol*. 2020;45(7):1973-1989.
4. Ma M, Yu B, Qin F, Yuan J. Current approaches to the diagnosis of vascular erectile dysfunction. *Transl Androl Urol*. 2020;9(2):709-721.
5. Cho MC, Song WH, Paick J. Suppression of cavernosal fibrosis in a rat model. *Sex Med Rev*. 2018;6(4):572-582.
6. Hassanin AM, Abdel-Hamid AZ. Cavernous smooth muscles: innovative potential therapies are promising for an unrevealed clinical diagnosis. *Int Urol Nephrol*. 2020;52(2):205-217.
7. Resim S, Koluş E, Barut O, Yasir A, Hasan B. Ziziphus jujube ameliorated cavernosal oxidative stress and fibrotic processes in cavernous nerve injury-induced erectile dysfunction in a rat model. *Andrologia*. 2020;52(7):e13632.
8. Kogan MI, Todorov SS, Popov IV, et al. Morphogenesis of penile cavernous fibrosis in hypotestosteronemia: an experimental study. *Urology Herarld*. 2020;8(1):14-24.
9. Ismail EA, Younis SE, Ismail IY, El-Wazir YM, El-Sakka AI. Early administration of phosphodiesterase 5 inhibitors after induction of diabetes in a rat model may prevent erectile dysfunction. *Andrology*. 2020;8(1):241-248.
10. Sahan A, Akbal C, Tavukcu HH, et al. Melatonin prevents deterioration of erectile function in streptozotocin-induced diabetic rats via sirtuin-1 expression. *Andrologia*. 2020;52(9):e13639.
11. Macit C, Ustundag UV, Dagdeviren OC, Mercanoglu G, Woodman OL. The effects of calorie restriction and exercise on age-related alterations in corpus cavernosum. *Front Physiol*. 2020;11:45.
12. Ruscitti F, Ravanetti F, Donofrio G, et al. A multimodal imaging approach based on micro-CT and fluorescence molecular tomography for longitudinal assessment of bleomycin-induced lung fibrosis in mice. *J Vis Exp*. 2018;134:56443.
13. Schambach SJ, Bag S, Schilling L, Groden C, Brockmann MA. Application of micro-CT in small animal imaging. *Methods*. 2010;50(1):2-13.
14. Suttapreyasri S, Suapear P, Leepong N. The accuracy of cone-beam computed tomography for evaluating bone density and cortical bone thickness at the implant site: micro-computed tomography and histologic analysis. *J Craniofac Surg*. 2018;29(8):2026-2031.
15. Mah P, Reeves TE, McDavid WD. Deriving Hounsfield units using grey levels in cone beam computed tomography. *Dentomaxillofac Radiol*. 2010;39(6):323-335.
16. Juliana JM, Zanette I, Noël PB, Cardoso MB, Kimm MA, Pfeiffer F. Three-dimensional non-destructive soft-tissue visualization with X-ray staining micro-tomography. *Sci Rep*. 2015;5:14088.
17. Bankhead P, Loughrey MB, Fernández JA, et al. QuPath: open source software for digital pathology image analysis. *Sci Rep*. 2017;7(1):16878.
18. Spani F, Morigi MP, Bettuzzi M, Scalici M, Carosi M. A 3D journey on virtual surfaces and inner structure of ossa genitalia in primates by means of a non-invasive imaging tool. *PLoS One*. 2020;15(1):e0228131.
19. O'Neill M, Huang GO, Lamb DJ. Novel application of micro-computerized tomography for morphologic characterization of the murine penis. *J Sex Med*. 2017;14(12):1533-1539.
20. Simopoulos DN, Gibbons SJ, Malysz J, et al. Corporeal structural and vascular micro architecture with X-ray micro computerized tomography in normal and diabetic rabbits: histopathological correlation. *J Urol*. 2001;165(5):1776-1782.
21. Kogan MI, Popov IgV, Popov IIV, Todorov SS. Penile cavernous fibrosis: etiology, morphogenesis, erectile dysfunction. *Urologiia*. 2020;4:144-150.
22. Glueckert R, Johnson Chacko L, Schmidbauer D, et al. Visualization of the membranous labyrinth and nerve fiber pathways in human and animal inner ears using microCT imaging. *Front Neurosci*. 2018;12:501.
23. Walton LA, Bradley RS, Withers PJ, et al. Morphological characterisation of unstained and intact tissue micro-architecture by X-ray computed micro- and nano-tomography. *Sci Rep*. 2015;5:10074.
24. Luangkhot R, Rutchik S, Agarwal V, Puglia K, Bhargava G, Melman A. Collagen alterations in the corpus cavernosum of men with sexual dysfunction. *J Urol*. 1992;148:467-471. Pt 1.
25. Ren P, Sun F, Li H-H. Dynamic changes in type and distribution of collagen fiber during albuginea penis healing using Picric-sirius red polarized light method. *J Clin Rehab Tis Engineer Res*. 2009;13(11):2187-2190.
26. de Souza DB, Silva D, Cortez CM, Costa WS, Sampaio FJ. Effects of chronic stress on penile corpus cavernosum of rats. *J Androl*. 2012;33(4):735-739.
27. Qian SQ, Qin F, Zhang S, et al. Vacuum therapy prevents corporeal veno-occlusive dysfunction and penile shrinkage in a cavernosal nerve injured rat model. *Asian J Androl*. 2020;22(3):274-279.
28. Raviv G, Vanegas JP, Petein M, et al. Biochemical alterations of the tunica albuginea in impotence. *J Urol*. 1997;158(5):1778-1782.
29. Sangiorgi G, Cereda A, Benedetto D, et al. Anatomy, pathophysiology, molecular mechanisms, and clinical management of erectile dysfunction in patients affected by coronary artery disease: a review. *Biomedicines*. 2021;9(4):432.
30. Moreland RB. Is there a role of hypoxemia in penile fibrosis: a viewpoint presented to the society for the study of impotence. *Int J Impot Res*. 1998;10(2):113-120.
31. El-Sakka AI, Yassin AA. Amelioration of penile fibrosis: myth or reality. *J Androl*. 2010;31(4):324-335.

32. Hodžić A, Ristanović M, Zorn B, et al. Genetic variation in leptin and leptin receptor genes as a risk factor for idiopathic male infertility. *Andrology*. 2021;5(1):70-74.
33. Cabrini MR, Sezen SF, Lagoda G, et al. Fibrotic protein expression profiles in penile tissue of patients with erectile dysfunction. *Urology*. 2013;82(4):975.e1-975.e6.
34. Hall A, Sherlock E, Sykes D. Does micro-CT scanning damage DNA in museum specimens? *J Nat Sci Collect*. 2015;2:22-28.
35. Webster JD, Miller MA, Dusold D, Ramos-Vara J. Effects of prolonged formalin fixation on diagnostic immunohistochemistry in domestic animals. *J Histochem Cytochem*. 2009;57(8):753-761.
36. Wang XJ, Xu TY, Xia LL, et al. Castration impairs erectile organ structure and function by inhibiting autophagy and promoting apoptosis of corpus cavernosum smooth muscle cells in rats. *Int Urol Nephrol*. 2015;47(7):1105-1115.
37. Parsa A, Ibrahim N, Hassan B, Motroni A, Van Der Stelt P, Wismeijer D. Reliability of voxel gray values in cone beam computed tomography for preoperative implant planning assessment. *Int J Oral Maxillofac Implant*. 2012;27(6):1438-1442.
38. Shokri A, Ghanbari M, Maleki FH, Ramezani L, Amini P, Tapak L, Relationship of gray values in cone beam computed tomography and bone mineral density obtained by dual energy X-ray absorptiometry. *Oral Surg Oral Med Oral Pathol Oral Radiol*. 2019;128(3):319-331.
39. Sadyrin E, Swain M, Mitrin B, et al. Characterization of enamel and dentine about a white spot lesion: mechanical properties, mineral density, microstructure and molecular composition. *Nanomaterials*. 2020;10(9):E1889.
40. Zou ZJ, Liang JY, Liu ZH, Gao R, Lu YP. Low-intensity extracorporeal shock wave therapy for erectile dysfunction after radical prostatectomy: a review of preclinical studies. *Int J Impot Res*. 2018;30(1):1-7.
41. Yang J, Yu Z, Zhang Y, et al. Preconditioning of adipose-derived stem cells by phosphodiesterase-5 inhibition enhances therapeutic efficacy against diabetes-induced erectile dysfunction. *Andrology*. 2020;8(1):231-240.
42. Tkachev SY, Mitrin BI, Karnaukhov NS, et al. Visualization of different anatomical parts of the enucleated human eye using X-ray micro-CT imaging. *Exp Eye Res*. 2021;203:108394.
43. Müller M, Kimm MA, Ferstl S, et al. Nucleus-specific X-ray stain for 3D virtual histology. *Sci Rep*. 2018;8(1):17855.
44. Pichat J, Iglesias JE, Yousry T, Ourselin S, Modat M. A survey of methods for 3D histology reconstruction. *Med Image Anal*. 2018;46:73-105.
45. Kavkova M, Zikmund T, Kala A, et al. Contrast enhanced X-ray computed tomography imaging of amyloid plaques in Alzheimer disease rat model on lab based micro CT system. *Sci Rep*. 2021;11(1):5999.
46. Holbrook M, Clark DP, Badea CT. Low-dose 4D cardiac imaging in small animals using dual source micro-CT. *Phys Med Biol*. 2018;63(2):025009.
47. Borland SJ, Behnsen J, Ashton N, et al. X-ray micro-computed tomography: an emerging technology to analyze vascular calcification in animal models. *Int J Mol Sci*. 2020;21(12):4538.
48. Mecozzi L, Mambrini M, Ruscitti F, et al. In-vivo lung fibrosis staging in a bleomycin-mouse model: a new micro-CT guided densitometric approach. *Sci Rep*. 2020;10(1):18735.

How to cite this article: Kogan MI, Popov IV, Kirichenko EY, et al. X-ray micro-computed tomography in the assessment of penile cavernous fibrosis in a rabbit castration model. *Andrology*. 2021;9:1467–1480. https://doi.org/10.1111/andr.13077